A Raman microprobe study of natural micas

A. TLILI, D. C. SMITH

Laboratoire de Minéralogie, Muséum National d'Histoire Naturelle, 61 rue de Buffon, 75005 Paris, France

J.-M. BENY

CNRS-CRSCM, 1A rue de la Férollerie, 45071 Orléans, France

AND

H. BOYER

ISA Jobin-Yvon, 16–18 rue du Canal, 91160 Longjumeau, France

Abstract

A wide range of natural K-, Na-, Ca- or (K + Li)-micas have been systematically examined by Raman spectrometry. The spectra are interpretable in terms of regular variations in peak positions and chemical parameters. Several vibrations give higher wavenumbers for Na-micas compared to K-micas, in accord with the smaller ionic size of Na^+ than K^+. The $\approx$195 cm^{-1} and $\approx$270 cm^{-1} peak wavenumbers and intensities vary as functions of the chemistry of the octahedral sites, i.e. the replacement of Mg^{2+} by Mn^{2+}, Zn^{2+}, Cr^{3+}, Fe^{3+}, Ti^{4+}, and especially by Al^{3+}, or by a vacancy, and the replacement of $(OH)^-$ by F^-. The group of $\approx$700 cm^{-1} peaks vary in wavenumber and intensity with the replacement of Si by Al in the tetrahedra; distinct Si–O–Si and Si–O–Al vibrations can be recognized. Di- and tri-octahedral micas are distinguished on the basis of certain relative peak intensities which vary considerably with polarization direction, and of trends with increasing $Al^{(iv)}$, $Al^{(vi)}$ or $Al^{(tot.)}$. Calibration of these trends for the chemical analysis of mica microinclusions seems feasible once the uncertainties in the data set are resolved by the determination of further samples selected to highlight the effect of specific elements.

KEYWORDS: Raman spectrometry, micas, phyllosilicates, crystal-chemistry, crystal physics.

Introduction

Previous work. Most studies of the vibrational spectra of micas presented during the last few years have concerned infrared spectroscopy (e.g. Farmer and Velde, 1973; Farmer, 1974; Velde, 1978; Langer *et al.*, 1981; see also the review by Rossman, 1984). Despite the pioneering work of Loh (1973), who presented some Raman spectra of micas and other phyllosilicates, micas were until recently considered to yield weak non-exploitable Raman spectra in contrast to minerals such as garnets (e.g. Moore and White, 1971; Boyer *et al.*, 1988), pyroxenes (e.g. Délé-Dubois *et al.*, 1980; Ohashi and Sekita, 1982, 1983), coesite (e.g. Boyer and Smith, 1984; Boyer *et al.*, 1985*a*), amphiboles (e.g. White, 1975; Smith and Boyer, 1987), titanates including titanite (Boyer *et al.*, 1985*b*) and geikielite–ilmenite–pyrophanite (Pinet *et al.*, 1987) or silicates in general (e.g. Griffith, 1975). Some data on muscovite and phlogopite were respectively given by Haley *et al.* (1982) and Clemens *et al.* (1987). Indeed as late as 1986, White (1986) emphasized the poor Raman response of micas.

This paper presents work on several natural di- and tri-octahedral (K, Na, Ca)-micas which shows that micas can indeed be thoroughly respectable minerals for Raman spectroscopic work (cf. Smith *et al.*, 1987; Tlili *et al.*, 1987). These micas are dominated by (Mg, Fe, Al) and (Si, Al) in the octahedral and tetrahedral sites respectively, but some varieties containing minor Mn, Zn, Cr, Fe and Ti were also included as well as two (K + Li)-micas.

Following a recapitulation of the essential features of crystal structure and chemical compo-

Mineralogical Magazine, April 1989, Vol. 53, pp. 165–79

sition of micas, the sample descriptions and the experimental methods, the general features of the Raman spectra of micas in the ranges of 50–1250 and 3500–3750 cm^{-1} are presented, with attention focused on the differences between trioctahedral and dioctahedral micas and between K-, Na-, Ca- and (K + Li)-micas, and on apparent trends of variation of each major Raman peak.

Crystal structure of micas: the essential features. Micas are composed of an octahedral sheet of (Mg, Fe, Al, etc.) cations sandwiched between the apical oxygens of two facing tetrahedral sheets of linked (Si, Al)O_4 tetrahedra: a so-called 2:1 layer phyllosilicate. Three 'bridging' or 'basal' oxygens of each tetrahedra form a hexagonal mesh pattern parallel to the mica cleavage whereas the fourth 'apical' oxygen points in the direction nearly perpendicular to the cleavage plane (crystallographic *a–b* plane). These apical oxygens form a hexagonal ring pattern with an (OH) ion in the centre; the hexagons of the two facing sets of apical oxygens + (OH) ions are coordinated by two octahedral cations in 'dioctahedral' micas or by three cations in 'trioctahedral' micas. Four apical oxygens and two (OH) groups contribute to form each octahedral site which can be occupied by tetravalent (Ti), trivalent (Al, Fe, Cr etc.), divalent (Mg, Mn, Fe, Zn etc.) or monovalent (Li) cations, or can be vacant; (OH) may be replaced by F.

The hydroxyl groups occur at the same *c*'-level as the apical oxygens and are directly linked to the structure only by one end (the oxygen), the other end (the hydrogen) being free to move according to the type of surrounding interactions. Vedder (1964) pointed out three types of orientation of the hydroxyl groups: *N*-type (normal), *I*-type (impurity), *V*-type (vacancy). In this classification 'normal' denotes three identical divalent octahedral cations (e.g. Mg Mg Mg), 'impurity' denotes two divalent plus one trivalent or monovalent cation (e.g. Mg Mg Al), and 'vacancy' denotes two trivalent cations plus one vacancy (e.g. Al Al □). This nomenclature was consolidated by the models established by Robert and Kodama (1988) and Robert *et al.* (1987, 1988) based on the infrared and Raman wavenumbers of hydroxyl-stretching in micas.

The unequal ionic sizes and/or charges among the octahedral or tetrahedral cations necessitate structural modifications. The substitution of Si by Al significantly increases the size of the tetrahedral sites ($r_{Si} \approx 0.26$ Å, $r_{Al^{(iv)}} \approx 0.39$ Å; Shannon, 1976) and is partly responsible for a distortion which may be characterized by the value alpha (where alpha = ditrigonal rotation angle: Donnay *et al.*, 1964; Robert, 1981). In the same way the substitution of Mg by Al ($r_{Mg} \approx 0.72$ Å, $r_{Al^{(vi)}} \approx 0.53$Å) substantially decreases the size of the octahedral sites and the presence of such an 'impurity' as Al in the octahedral site accounts for the distortion in trioctahedral micas compared to pure phlogopite.

Two tetrahedral sheets are joined back-to-back by 'interlayer' cations of low valency (K, Na or Ca) which serve to balance the net negative charges of the 2:1 tetrahedral : octahedral layers. In $Al^{(iv)}$-poor K-micas the two patterns of hexagonally-arranged bridging oxygens are almost exactly superposed, and all the bridging oxygens on each side are almost coplanar, giving rise to coordination 12 for K^+. In Na-micas, the smaller interlayer cation considerably distorts the geometry of the bridging oxygens by tilting and rotating the tetrahedra. Likewise $Al^{(iv)}$ substitution into the tetrahedra of K- or Na-micas distorts the fitting together of the opposing tetrahedral sheets. In margarite, the tetrahedral distortion results in coordination 6 for the Ca atoms, with a distinct shifting along the cleavage plane of the opposing pseudo-hexagonal tetrahedral patterns. For further details the reader is referred to review articles by Zussman (1979), Bailey (1984*a* and *b*), and Guggen heim (1984) and the many references cited therein.

Chemical composition of micas: the essential features. Setting aside the Ca- and (K + Li)-micas and the minor elements such as Mn^{2+}, Zn^{2+}, Ba^{2+}, Cr^{3+}, V^{3+} and Ti^{4+}, and combining Fe^{2+} with Mg, Fe^{3+} with Al and any F or Cl with (OH), reduces the chemistry of natural rock-forming (K,Na)-micas to the system K–Na–Mg–Al–Si–O–H and gives the simplified formula:

$$(K, Na)_2Mg_{0-6}Al^{(vi)}_{0-4}\square_{0-2}Si_{4-8}Al^{(iv)}_{0-4}O_{20}(OH)_4,$$

where □ denotes an octahedral vacancy.

Many ways of plotting mica compositions have been published and all have various advantages and disadvantages. Here we use the '$Al^{(vi)}$ *vs.* $Al^{(iv)}$ mica hexagon' of Smith (1988) where only $Al^{(iv)}$ and $Al^{(vi)}$ are plotted such that $Al^{(tot.)}$ increases horizontally to the right as (Mg + Si) decreases, the total number of Mg cations being implicitly fixed if (K + Na) = 2 and (OH) = 4 (Fig. 1).

Ca-micas ('brittle micas') require greater Al and/or greater vacancy contents to maintain overall charge balance. Margarite is thus related to paragonite by the exchange $Ca_2Al^{(iv)}_2 = Na_2Si_2$, and to preiswerkite by the exchange $Ca_2Al^{(vi)}_2\square_2 = Na_2Mg_4$. Li can enter the octahedral site of K-, Na- or Ca-micas and the charge can be balanced in several ways, e.g. trilithionite is related to phlogopite by the exchange $Mg_6 = Li_3Al_3$.

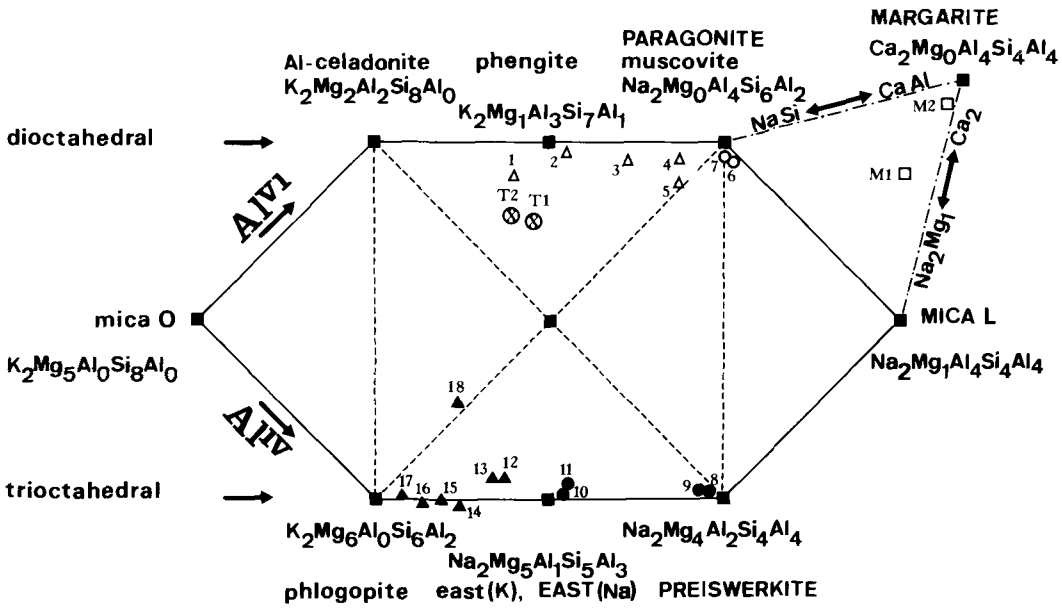

FIG. 1. Plot of sample chemical compositions (data of Tables 2 and 3) on the 'mica hexagon' of Smith (1988) in order of increasing $Al^{(tot.)}$ for dioctahedral micas and decreasing $Al^{(tot.)}$ for trioctahedral micas; the coordinates are $Al^{(iv)}$ and $Al^{(vi)}$ for the hexagon and $Al^{(iv)}$ and Ca for the margarite–paragonite–'MICA L' triangle which may be visualized as being perpendicular to the hexagon. K-micas in small print; Na- or Ca- micas in capitals. $O_{20}(OH, F)_4$ throughout. Na includes K; Mg includes Fe, Mn, Ni; $Al^{(vi)}$ includes Cr. △, dioctahedral (K)-micas; ▲, trioctahedral (K)-micas; ○, dioctahedral (Na)-micas; ●, trioctahedral (Na)-micas; □, margarite; ⊗, trilithionite; ■, ideal end-members.

Replacement of Mg by Fe^{2+} and/or of $Al^{(vi)}$ by Fe^{3+} is extensive and affects mica stability and hence also the limits of natural solid-solution ranges.

The 22 micas studied here by the electron microprobe and Raman microprobe techniques are plotted in Fig. 1; they represent most of the known natural composition ranges corresponding to the formula given above but with $Mg > Fe^{2+}$ and $Al > Fe^{3+}$.

Data acquisition

Sample origins and compositions. The mica samples studied here come from a variety of localities and geological environments (Table 1). Electron microprobe analyses are presented in Tables 2 and 3; these were determined with a CAMECA CAMEBAX microprobe at the Paris Museum (see Smith and Pinet, 1985, for the operational details). In the dioctahedral micas, where $Fe^{(tot.)}$ and $Mn^{(tot.)}$ are low, all Fe and Mn are presented as Fe^{2+} and Mn^{2+} since most total weight percent values exceed 100%. Since most of the Fe-richer trioctahedral micas have total weight percent values close to 100% and most Σalk. and Σoct. values are reasonable, then $Fe^{(tot.)}$ is also left as Fe^{2+}. The real Fe^{3+} and Mn^{3+} values are probably as small as the Cr^{3+} values, except for sample 1 (Table 1), and may be ignored without introducing significant error into the calculated total trivalent occupancy of the octahedra.

Raman microprobe experimental technique. The crystals were either mounted in a cylinder of Araldite or glued with Araldite to a glass slide and then polished; the same mounts, and indeed exactly the same crystals, were used for both the electron microprobe and Raman microprobe analyses.

The Raman spectra were recorded with the electric field polarized either parallel or perpendicular to the cleavage plane. Near identical Raman microprobes at CNRS-CRSCM (Orléans) and ISA JOBIN-YVON (Longjumeau) were used. Both were composed of a RAMANOR U1000 microspectrometer equipped with an OLYMPUS microscope and an INNOVA-90 argon ion laser; the slits were set at 200–400 μm. The exciting line was usually at $\lambda = 514.5$ nm (green) but sometimes at $\lambda = 488$ nm (blue). Estimated errors were $\pm 1\ cm^{-1}$ in precision and $\pm 2\ cm^{-1}$ in accuracy for those peaks which are strong and without

Table 1.
Sample descriptions

N°	SPECIES	ROCK	LOCALITY	COUNTRY
	DIOCTAHEDRAL (K,Na)-MICAS INCLUDING MARGARITE			
1	phengite (Mn) 'alurgite'	N4	St. Marcel	Italy
2	phengite	1131	Weissenstein	Germany
3	phengite	FTS4	Oberkotzau	Germany
4	muscovite	A58	Hessdalen	Norway
5	muscovite (Cr) 'fuchsite'	GAL 170-39		Madagascar
6	paragonite	G193	Liset	Norway
7	paragonite	G193	Liset	Norway
M1	margarite (Na)	K26	Liset	Norway
M2	margarite	93by	Rekvika	Norway
	TRIOCTAHEDRAL (K,Na)-MICAS INCLUDING TRILITHIONITE			
8	preiswerkite	G184	Liset	Norway
9	preiswerkite	G184	Liset	Norway
10	east(Na)*	K27	Liset	Norway
11	east(Na)*	K27	Liset	Norway
12	east(K)* (Ti)	A70	Hessdalen	Norway
13	east(K)*	B331b	Aarsheimneset	Norway
14	phlogopite	GAL 130-251		Madagascar
15	phlogopite	GAL 112-243	Arendal	Norway
16	phlogopite (F)	GAL 168-7		Brazil
17	hendricksite (Ba,Ti) £	M-7	Franklin Furnace	U.S.A.
18	annite (Ti)	HEL 697	Sierra los Filabres	Spain
T1	trilithionite (Mn)	GAL 152-85	Erajanic	Finland
T2	trilithionite (Mn)	GAL 152-85	Erajanir	Finland

*: The name 'eastonite' for the K end-member has recently been discredited by Livi and Veblen (1987), and the Na end-member has not yet been recognised by the IMA commission on New Minerals and Mineral Names; here we use the symbols 'east(Na)' and 'east(K)' to indicate those compositions close to $(K,Na)_2(Mg,Fe)_5Al_2Si_5Al_3O_{20}(OH)_4$ with respectively Na > K or K > Na .
Elements other than K, Na, Ca, Li, Mg, Fe, Al, Si, O, H, are indicated in brackets where their contents are significant.
Sample 17 was kindly provided by Dr. J.-L. Robert and X-ray refined by Robert and Gaspérin (1985).
£: Hendricksite is an (Mn + Zn)-bearing phlogopite.

shoulders. The number of scans, counting times, laser power and wavenumber steps all varied somewhat as these samples were determined during different RMP sessions spread over several years.

Despite frequently successfully obtaining spectral data, some technical obstacles were encountered when recording mica samples (e.g. high background noise, high fluorescence or strong absorption). Especially when the crystals are Fe^{2+}-rich, the incident monochromatic light, whether focused or defocused, is strongly absorbed by the sample which can become damaged by heating at the impact point. However, in general the quality of the Raman spectra is not significantly affected by the colour (i.e. the wavelength ranges of absorption), but it is dependent on the transparency of the material (i.e. the total absorption). Thus red 'alurgite' (manganian phengite), green 'fuchsite' (chromian muscovite), brown phlogopite and pink trilithionite yield spectra as strong as those of colourless muscovite and paragonite which in turn are comparable in intensity to the Raman spectra of pyroxenes and amphiboles.

General features of the Raman spectra of micas

Peak assignments. The expected wavenumbers for Raman and infrared vibrations have been calculated using a factor group analysis procedure based on the GF matrix method (Shimanouchi *et al.*, 1961; Ishii *et al.*, 1967, 1969). Loh (1973) attributed the Raman active vibrational bands in micas and other phyllosilicates to molecular vibrations of MO_6, SiO_4, O–H–O and O–H. Velde and Couty (1985) based their infrared band attributions in certain phyllosilicates on the variation of spectra with chemical composition, i.e. on different cation substitutions in various sites for simi-

Table 2.
Electron probe analyses of natural dioctahedral (K,Na)-micas including margarite

sample	1*	2	3	4	5	6	7	M1	M2
SiO2	52.80	51.81	49.10	46.27	44.83	45.63	46.75	32.83	30.74
Al2O3	21.07	27.70	31.48	34.80	34.70	40.30	40.19	49.36	50.14
Cr2O3	0.00	0.01	0.00	0.20	0.92	0.00	0.00	0.01	0.00
FeO	1.83	2.26	0.54	1.87	1.38	0.41	0.16	1.18	0.32
MnO	1.80	0.02	0.00	0.06	0.00	0.00	0.00	0.01	0.00
MgO	5.82	3.45	3.41	0.51	1.62	0.12	0.37	1.02	0.49
TiO2	0.21	0.72	0.46	0.33	0.53	0.26	0.17	0.01	0.00
K2O	12.29	11.16	10.58	11.05	11.27	0.21	0.11	0.02	0.00
Na2O	0.01	0.61	0.80	0.54	0.55	7.60	7.20	3.95	1.20
CaO	0.00	0.00	0.00	0.00	0.00	0.47	0.66	7.05	12.22
H2O	4.43	4.58	4.56	4.49	4.47	4.67	4.72	4.55	4.50
TOTAL	100.26	102.32	100.95	100.12	100.27	99.67	100.33	99.99	99.61
Si	7.068	6.765	6.444	6.180	6.007	5.855	5.936	4.320	4.089
Al(tot)	3.324	4.264	4.870	5.477	5.480	6.096	6.015	7.657	7.860
Al(iv)	0.932	1.235	1.556	1.820	1.993	2.145	2.064	3.680	3.911
Σtet	8.000	8.000	8.000	8.000	8.000	8.000	8.000	8.000	8.000
Al(vi)	2.392	3.029	3.314	3.657	3.487	3.951	3.951	3.977	3.949
Cr	0.000	0.000	0.000	0.021	0.097	0.000	0.000	0.001	0.000
Fe(tot)	0.204*	0.248	0.059	0.206	0.154	0.045	0.017	0.129	0.035
Mn	0.204*	0.002	0.000	0.006	0.000	0.000	0.000	0.001	0.000
Mg	1.162	0.672	0.668	0.102	0.324	0.023	0.069	0.201	0.097
Ti	0.020	0.071	0.046	0.033	0.053	0.025	0.016	0.001	0.000
Σoct.	3.982	4.022	4.087	4.025	4.115	4.044	4.053	4.309	4.081
K	2.099	1.859	1.771	1.882	1.927	0.034	0.017	0.003	0.000
Na	0.003	0.154	0.205	0.139	0.144	1.892	1.772	1.008	0.310
Ca	0.000	0.000	0.000	0.000	0.000	0.064	0.090	0.994	1.742
Σalk.	2.102	2.013	1.976	2.021	2.071	1.990	1.879	2.005	2.052
OH	4.000	4.000	4.000	4.000	4.000	4.000	4.000	4.000	4.000
F	n.d.	n.d.	n.d.	n.d.	n.d.	n.d.	n.d.	n.d.	n.d.
TOTAL	18.084	18.035	18.063	18.046	18.186	18.034	17.932	18.315	18.134

Cations on the basis of 44 total charges; OH = 4 by assumption; H_2O by calculation; n.d. = not determined.
Analysis n°2 from Franz et al. (1986).
* : Trivalent Fe and Mn instead of divalent, following Knurr and Bailey (1986).

lar types of sheet silicate. Likewise in this study, Raman spectra are interpreted with reference to certain crystal-chemical features of dioctahedral and trioctahedral micas; in particular the charge balance in the octahedra and tetrahedra and the O–H orientation.

As shown in Table 4 and Fig. 2*a* and *b*, which display a selection of example spectra, natural micas yield a variety of peaks in the 50–1250 and 3500–3750 wavenumber regions, most of which are in agreement with those reported by Loh (1973) for natural lepidolite, muscovite, phlogopite, and margarite, and by Clemens *et al.* (1987) for synthetic phlogopite. The data reported by Haley *et al.* (1982) on the (OH) vibration of 'clay muscovite' do not fit with our data nor with that of Loh (1973); we thus suspect that their clay muscovite is not a true muscovite. In order to simplify the discussion the spectra are sub-divided as follows:

low wavenumber region = 50–300 cm^{-1}
high wavenumber region = 300–1250 cm^{-1}
OH-stretching region = 3500–3750 cm^{-1}

Low wavenumber region (50–300 cm^{-1}). The Raman spectra of micas show several peaks in this region: ≈100 cm^{-1}, ≈160 cm^{-1} (rarely), ≈195 cm^{-1}, ≈220 cm^{-1}, ≈240 cm^{-1} (rarely), and ≈270 cm^{-1}. Loh (1973) assigned those peaks below 230 cm^{-1} to the internal vibrations of the MO_6 octahedron. Ishii *et al.* (1967) had assigned most infrared bands in this region to vibrations involving the interlayer cation. However, Raman spectra of talc reported by Loh (1973) and Rosasco and Blaha (1980) yield the same 100 cm^{-1} peak as the micas despite the absence of an interlayer cation. The ≈100 cm^{-1} peak can be strong in both di- and tri-octahedral micas, but is frequently hidden by the noise and the exciting line in our spectra; its wavenumber varies somewhat irregularly with the chemical composition of micas (Table 4).

The ≈195 cm^{-1} peak is strong in dioctahedral micas; it is the strongest peak in trioctahedral micas when the electric field is orientated perpendicular to the cleavage plane, but it becomes weak when the electric field is parallel to the cleavage plane. The peak position increases in wave-

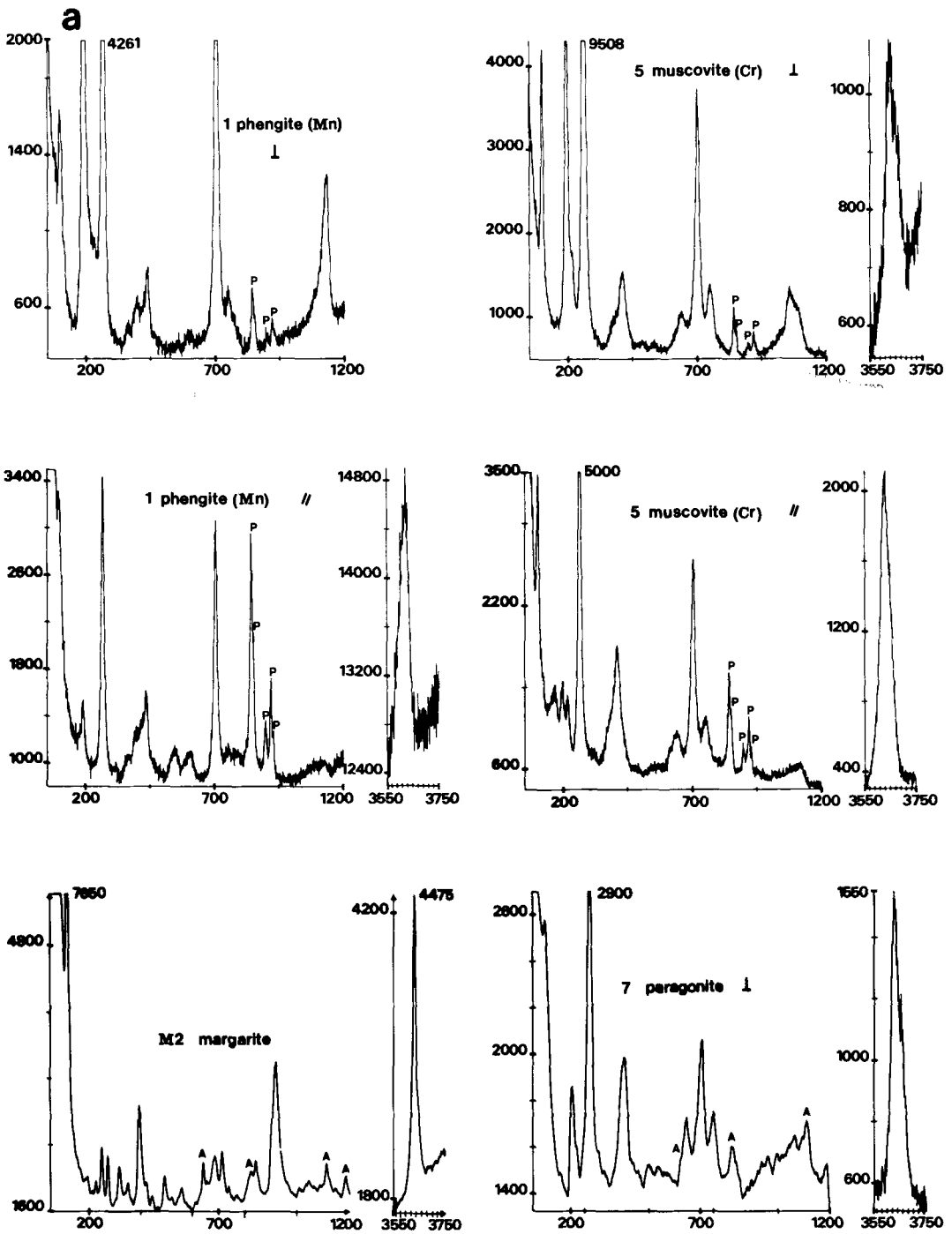

FIG. 2. Selected Raman spectra: (a) dioctahedral (K, Na)-micas including margarite; (b) trioctahedral (K, Na)-micas including trilithionite. Sample numbers as in Table 1. // and ⊥ indicate incident laser polarization parallel or perpendicular to the cleavage plane. A denotes a peak of Araldite. P denotes a parasite due to the microscope objective. The abscissa is the Raman shift in cm^{-1}. The intensity scale is in total counts; the intensity of off-scale peaks is noted alongside.

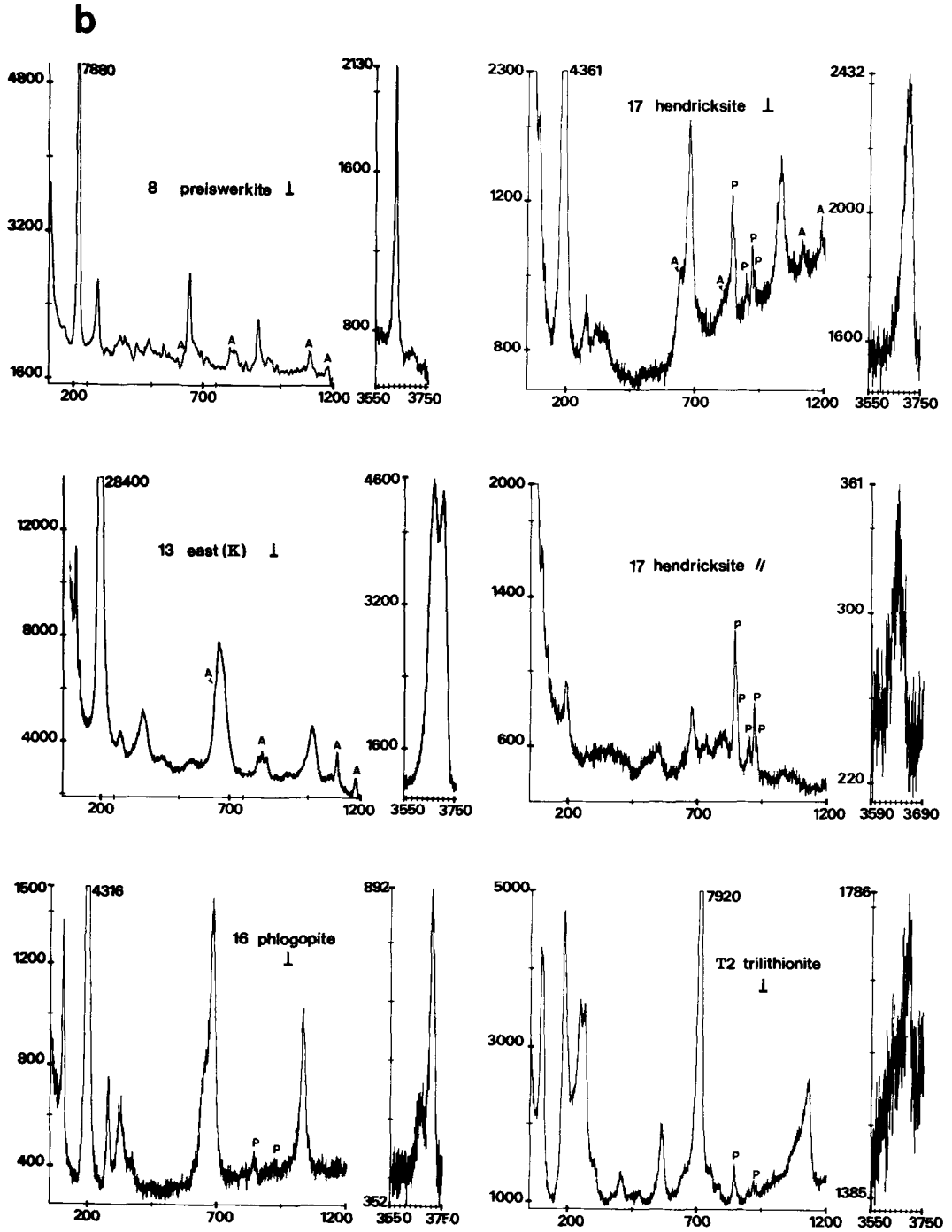
b
8 preiswerkite ⊥
17 hendricksite ⊥
13 east (K) ⊥
17 hendricksite //
16 phlogopite ⊥
T2 trilithionite ⊥

Table 3.
Electron probe analyses of natural trioctahedral (K,Na)-micas including trilithionite.

sample	8	9	10	11	12	13	14	15	16	17	18	T1	T2
SiO2	30.06	30.29	35.06	35.90	36.75	37.74	38.37	37.40	40.88	37.53	38.87	49.47	51.04
Al2O3	35.91	35.46	25.67	25.86	19.87	20.40	17.05	15.87	14.93	12.44	16.48	24.19	23.32
Cr2O3	0.00	0.00	0.00	0.12	0.00	0.00	0.00	0.00	0.02	0.15	0.01	0.07	0.05
FeO	5.90	6.53	7.93	7.42	16.24	10.32	3.69	11.82	1.15	3.94	24.84	3.33	3.02
MnO	0.00	0.00	0.09	0.16	0.16	0.00	0.00	0.40	0.12	6.03	0.09	1.92	1.90
MgO	16.30	16.45	18.66	18.33	11.02	18.23	24.03	18.44	26.88	13.48	1.36	0.01	0.04
NiO	0.00	0.00	0.12	0.00	0.00	0.00	0.00	0.00	0.09	0.00	0.00	0.00	0.00
ZnO	n.d	n.d	n.d	n.d	n.d	n.d	n.d.	n.d.	n.d.	9.36	n.d.	n.d.	n.d.
TiO2	0.00	0.06	0.66	0.59	2.62	0.17	1.02	0.09	0.12	1.13	4.13	0.00	0.02
Li2O	n.d.	n.d.	n.d.	n.d.	n.d.	n.d.	n.d.	n.d.	n.d.	n.d.	n.d.	5.78*	5.68*
K2O	0.06	0.04	0.46	0.32	9.32	8.29	10.95	10.56	10.97	8.98	9.29	11.22	11.07
Na2O	7.53	7.57	6.85	7.26	0.33	1.22	0.37	0.17	0.26	0.64	0.00	0.40	0.34
CaO	0.60	0.03	0.01	0.01	0.00	0.00	0.00	0.00	0.00	0.00	0.03	0.00	0.00
BaO	n.d.	n.d.	n.d.	n.d.	n.d.	n.d.	n.d.	n.d.	n.d.	1.28	n.d.	n.d.	n.d.
H2O	4.36	4.38	4.30	4.34	4.06	4.20	4.05	3.76	3.16	3.90	3.34	4.49	4.54
F	n.d.	n.d.	n.d.	n.d.	0.00	n.d.	0.35	0.55	2.36	n.d.	1.12	n.d	n.d
TOTAL	100.72	100.81	99.81	100.31	100.37	100.57	99.69£	98.83£	99.95£	98.88	99.09£	100.88	101.02
Si	4.127	4.140	4.880	4.953	5.426	5.388	5.457	5.574	5.736	5.840	6.024	6.603	6.740
Al(tot)	5.810	5.714	4.211	4.205	3.458	3.434	2.858	2.788	2.469	2.300	3.010	3.806	3.629
Al(iv)	3.873	3.860	3.120	3.047	2.574	2.612	2.543	2.426	2.264	2.160	1.976	1.397	1.260
Σtet	8.000	8.000	8.000	8.000	8.000	8.000	8.000	8.000	8.000	8.000	8.000	8.000	8.000
Al(vi)	1.937	1.854	1.091	1.158	0.884	0.822	0.315	0.362	0.205	0.140	1.034	2.409	2.369
Cr	0.000	0.000	0.000	0.013	0.000	0.000	0.000	0.000	0.002	0.020	0.001	0.007	0.005
Fe(tot)	0.677	0.746	0.923	0.856	2.005	1.233	0.439	1.473	0.135	0.500	3.220	0.371	0.332
Mn	0.000	0.000	0.011	0.018	0.020	0.000	0.000	0.050	0.015	0.800	0.012	0.217	0.215
Mg	3.336	3.352	3.871	3.769	2.425	3.879	5.094	4.098	5.621	3.140	0.314	0.002	0.008
Ni	0.000	0.000	0.014	0.000	0.000	0.000	0.000	0.000	0.010	0.000	0.000	0.000	0.000
Zn	n.d.	n.d.	n.d.	n.d.	n.d.	n.d.	n.d.	n.d.	n.d.	1.080	n.d.	n.d.	n.d.
Ti	0.000	0.006	0.068	0.060	0.291	0.018	0.109	0.010	0.012	0.140	0.482	0.000	0.001
Li	n.d.	n.d.	n.d.	n.d.	n.d.	n.d.	n.d.	n.d.	n.d.	n.d.	n.d.	2.994	3.069
Σoct.	5.950	5.958	5.978	5.874	5.625	5.952	5.957	5.993	6.000	5.820	5.063	6.000	6.000
K	0.009	0.007	0.081	0.055	1.745	1.509	1.989	2.007	1.963	1.780	1.837	1.885	1.865
Na	2.005	2.008	1.849	1.942	0.095	0.338	0.103	0.049	0.071	0.200	0.000	0.085	0.086
Ca	0.009	0.005	0.001	0.009	0.000	0.000	0.000	0.000	0.000	0.000	0.004	0.000	0.000
Ba	n.d.	n.d.	n.d.	n.d.	n.d.	n.d.	n.d.	n.d.	n.d.	0.080	n.d.	n.d.	n.d.
Σalk	2.023	2.020	1.931	2.006	1.840	1.847	2.092	2.056	2.034	2.060	1.841	1.970	1.951
OH	4.000	4.000	4.000	4.000	4.000	4.000	3.842	3.740	2.955	4.000	3.451	4.000	4.000
F	n.d.	n.d.	n.d.	n.d.	0.000	n.d.	0.158	0.260	1.045	n.d.	0.549	n.d.	n.d.
TOTAL	19.973	19.978	19.909	19.880	19.465	19.799	20.049	20.049	20.034	19.880	18.905	19.970	19.950

* = Li calculated by difference from 6 cations in the octahedral site;
Li_2O by calculation. OH and H_2O as in table 2, except by difference where F is analysed.
Analysis n° 17 from Robert and Gaspérin (1985).
£: O = 2F deducted.

number with increasing $Al^{(iv)}$ and with $Al^{(vi)}$ (Fig. 3*a* and *b*) in both di- and tri-octahedral (K, Na)-micas. This is compatible with Loh's (1973) interpretation that this peak involves the octahedral site since, for the same mineral group, Raman wavenumbers in general increase with decreasing bond lengths and here the smaller size and greater charge of Al^{3+} compared to Mg^{2+} reduce the mean octahedral cation–oxygen bond distance.

The ≈160 and ≈220 cm^{-1} peaks are weak or absent. The ≈220 cm^{-1} peak occurs only in dioctahedral micas and is stronger in margarite where it occurs at 225 cm^{-1} (cf. Loh, 1973) (Table 4). The ≈240 cm^{-1} peak becomes strong to medium only in trilithionite and margarite and was attributed by Loh (1973) to asymmetrical stretching of the 'isosceles triangle O–H–O' where the two oxygens are adjacent apical oxygens and not the oxygens of the (OH) group.

The ≈270 cm^{-1} peak occurs in all dioctahedral micas and trilithionite as a strong peak. It is weak in compositions close to phlogopite, but it becomes stronger in preiswerkite when the electric field is polarized perpendicular to the cleavage plane. Loh (1973) suggested that this peak occurs only in dioctahedral micas and 'lepidolite' (which both lack identical cations in each octahedral site) and involves symmetrical stretching of the isosceles triangle O–H–O composed of the proton and two adjacent apical oxygens. The presence of this peak in preiswerkite at higher wavenumber and intensity than the same peak in compositions near to phlogopite could be interpeted, as in dioctahedral micas, by the interaction of the proton with two apical oxygens because of the presence of impurities such as Al^{3+} in the octahedral sites

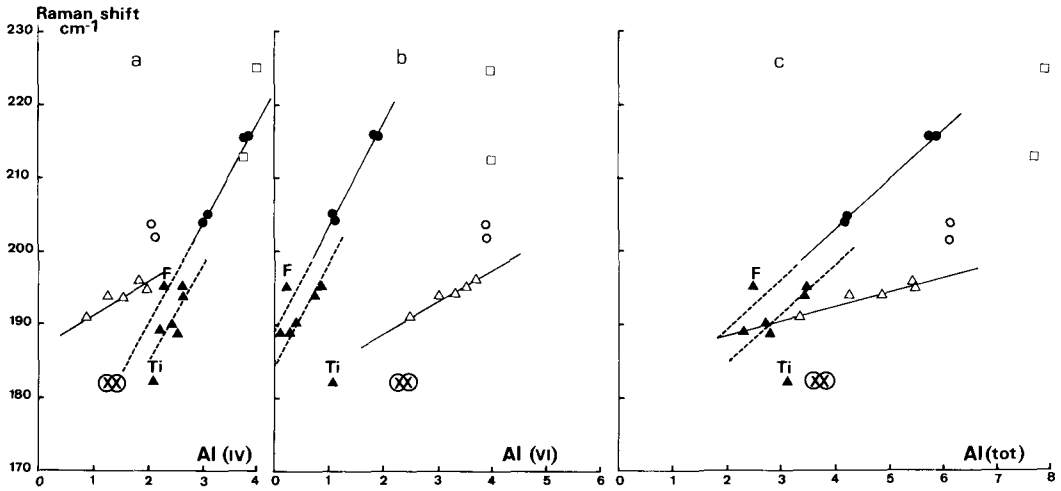

FIG. 3*a*, *b* and *c*. Trends of variation of the ≈195 cm^{-1} peak with $Al^{(iv)}$, $Al^{(vi)}$, and $Al^{(tot.)}$ respectively. Symbols as in Fig. 1. F- or Ti-rich samples are indicated. Solid and dashed lines represent 'probable' and 'possible' trends respectively. Vertical bars denote uncertainties in peak position for peaks that are weak, wide or composite.

whereby the different charge and/or size of the impurity cation moves the proton off-centre such that it interacts with the nearest apical oxygens (e.g. the two furthest from Al^{3+}).

The wavenumber of the ≈270 cm^{-1} peak decreases with increasing $Al^{(iv)}$ or increasing $Al^{(vi)}$ in dioctahedral K-micas but the situation in trioctahedral K-micas is less clear (Fig. 4*a* and *b*).

High wavenumber region (300–1250 cm^{-1}). Ishii *et al.* (1967, 1969) assigned the bands in this region to vibration of Si_2O_5 layers and (OH) librations. In contrast, the vibration bands in this region were interpreted by Loh (1973) as internal vibrations of the distorted SiO_4 tetrahedron. Van Der Marel and Beutelspacher (1976) and Langer *et al.* (1981) attributed infrared peaks in the 445–1162 cm^{-1} region in muscovite to vibrations of Si–O–Si, Si–O–Al, Al–O–Al, Si–O, Al–O and Al–OH, but differed in their specific attribution for several peaks.

The strong Raman peaks in this region occur between 640 and 715 cm^{-1}. The highest peak has a higher wavenumber and intensity in dioctahedral (K, Na)-micas and trilithionite than in trioctahedral (K, Na)-micas. These peaks involve tetrahedral sites, as also in the case of the peak occurring at ≈1040 cm^{-1} (e.g. 1028 in phlogopite; 1058 in muscovite), by analogy with the Raman spectra of pyroxenes (White, 1975; Ohashi and Sekita, 1982, 1983; Sharma *et al.*, 1983; Smith and Boyer, 1985) and the Raman spectra of amphiboles (White, 1975; Smith and Boyer, 1987). The peak at 702 cm^{-1} in muscovite and at 679 cm^{-1} in phlogopite is thus assigned to Si–O–Si vibrations. The dioctahedral micas and trilithionite yield a weak band at ≈640 and 650 cm^{-1} respectively, whereas Al-poor trioctahedral (K, Na)-micas yield a shoulder at ≈654 cm^{-1}. We recently suggested that the peak at 640 cm^{-1} in muscovite, 650 cm^{-1} in trilithionite, 654 cm^{-1} in phlogopite and 648 cm^{-1} in preiswerkite concerns Si–O–Al vibrations (Tlili *et al.*, 1988). The intensity of this peak increases with increasing $Al^{(tot.)}$ in trioctahedral micas and reaches a maximum in preiswerkite ($Al^{(iv)}$ = $Si^{(iv)}$ = 4), whilst the intensity of the Si–O–Si vibration decreases and becomes very weak in preiswerkite at ≈679 cm^{-1} where a similarly weak Al–O–Al occurs at 655 cm^{-1} (Tlili, Smith, Levoir and Aubard, in prep.).

Other peaks occurs at ≈325, ≈360, and ≈560 cm^{-1}, mainly in (K, Na)-trioctahedral micas, and a wide peak occupies the 400–435 cm^{-1} range, mainly in dioctahedral micas and trilithionite; the latter is due to the overlapping of the (OH) libration and Si–O vibration according to Loh (1973).

Spectra of margarite show a strong peak at 393 cm^{-1} and a very strong peak at 917 cm^{-1} and are thus quite different to those of (K-, Na- or K + Li)-micas; nevertheless they are consistent with the infrared data reported by Vedder and McDonald (1963), Naumann *et al.* (1966) and Langer *et al.* (1981) who suggested that these peaks involve (OH) libration, although another strong infrared peak at 925 cm^{-1} was attributed to Si–O–Al vibration by Van Der Marel and Beu-

Table 4.
Wavenumbers of Raman peaks in the ranges 50 - 1200 cm-1 and 3600 - 3750 cm-1

cm-1	1	2	3	4	5	6	7	M1	M2	8	9	10	11	12	13	14	15	16	17	18	T1	T2
50																						
100	100			(100)	100	100			84 115*		108				100	95	97	101	(94)		100	94
150																						
200	191*	194	194	196 (220)	166 195 218	202 220	204 220	213	(225)	216*	156 216*	205*	204*	195*	194*	189*	190*	195*	189*	182*	182	182
250									248		(280)			(263)							243	244
300	268	264*	266*	262*	263*	270*	272*	264*	271	292	292				(274)		273	276	(278)	(272)	260	260 (300)
350	(360)							310 365	315 (348)		330			(355)	361			327 (369)	(317) (331)			
400	(395)	(400)		(408)	386 410	392 410	406	391	393		(379) (400)	400	(395)	(400)	400						(406)	(405)
450	435	(426)	420						489 (553)		488											
500					485																	
550	(545)		(550)		533							542									558 (589)	561
600	(603)																					
650			(650)		639	645	646		648	648	648			654	652	652	650	654	644		(648)	(650)
700	705	704*	704	703	702	706	704	670 (712)	676 711		679	671	672	672	670	677	675	679	677	676	707*	707*
750	(751)	750		745	750	748	750														(750)	(750)
800																						
850																						
900																						
950								917	917	916	916		(918)									
1000													(1015)	1017	1014	(1006)	(1000)	(995)				
1050					1058			(1032)								(1039)	(1024)	1030	1028	(1045)		
1100	(1083)																				(1094)	(1094)
1150	1130																				1127	1128
1200																						
3600	3595							3632	3635	3620												
3650	3623		(3620)	3626	3628 3650		3628 3653			3628					3663	3658		3666		3658		
3700															3700			3709	3680 3700		3691	3691
3750																						

* = strongest, __ = strong to medium, without mark = weak, ( ) = very weak

telpacher (1976) and Langer *et al.* (1981). Margarite shows three peaks in the 640–715 cm^{-1} region which might represent Si–O–Al, Al–O–Al and Si–O–Si vibrations.

(OH)-stretching region (3500–3750 cm^{-1}). In this region the dioctahedral micas phengite, muscovite, paragonite and margarite yield a medium-intense peak at 3623, 3628, 3628, and 3635 cm^{-1} respectively; this peak in infrared spectra was interpreted by Vedder (1964) as a *V*-type stretching vibration of (OH) close to two trivalent cations and a vacant site. In dioctahedral micas this peak is generally very wide and some other extra vibrations occur; they manifest themselves as a shoulder e.g. in phengite at ≈3595 cm^{-1}, in muscovite at ≈3650 cm^{-1}.

The intensities of the main (OH) band in dioctahedral micas are particularly sensitive to the orientation of the sample under the laser beam: medium intensity when the electric field is parallel to the cleavage plane and weak when the electric field is perpendicular. Note that the O–H direction in dioctahedral micas is almost parallel (12° in 2*M*1 muscovite; Bailey, 1984*b*, p. 36; see also Tables 1 and 2 in Giese, 1984) to the cleavage plane due to the pushing off-vertical by the two higher-charged $Al^{(vi)}$ atoms.

In trioctahedral micas the Raman spectra of phlogopite yield a medium peak at 3709 cm^{-1} interpreted as an *N*-type stretching vibration of (OH) influenced by three divalent cations with O–H directed close to the *c'* axis (cf. Vedder,

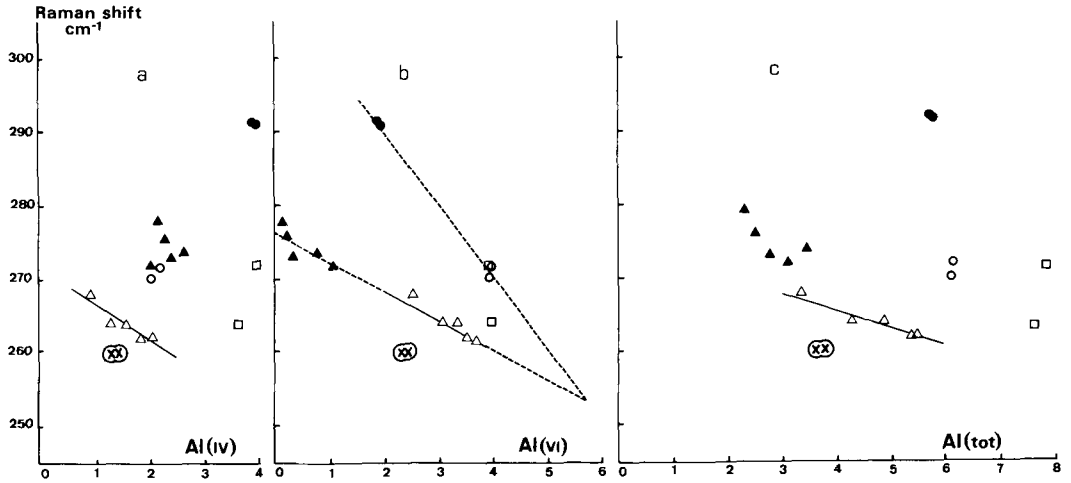

FIG. 4*a*, *b* and *c*. Trends of variation of the ≈270 cm^{-1} peak with $Al^{(iv)}$, $Al^{(vi)}$, and $Al^{(tot.)}$ respectively.

1964; Giese, 1984; Robert and Kodama, 1988). The presence of an 'impurity' such as Fe^{3+}, or Al^{3+} in the octahedral site moves the proton off-centre and yields a very weak *I*-type peak at ≈3666 cm^{-1} in compositions near to phlogopite.

East(K) and east(Na) yield two vibrations with a similar medium intensity at 3690 cm^{-1} and 3660 cm^{-1} interpreted as *N*-type and *I*-type vibrations respectively and occurring near to those reported by Robert and Kodama (1988) on synthetic East(K) recorded by infrared. Having an ideal octahedral composition of Mg_5Al_1, the proportions of (Mg, Mg, Mg) and (Mg, Mg, Al) bonded to an (OH) group should be equal.

Preiswerkite yields a peak with medium intensity at 3628 cm^{-1} and a very weak peak at 3690 cm^{-1}, believed to correspond to *I*-type and *N*-type respectively (cf. as reported by Liu *et al.*, 1987, and Robert and Kodama, 1988, for synthetic preiswerkite studied by infrared and Raman spectrometry). One other peak is detected at 3620 cm^{-1}, which may correspond to the stretching vibration of (OH) surrounded by (Mg, Mg, Fe).

The intensities of the *N*-type and *I*-type bands in trioctahedral micas are also sensitive to the orientation of the sample: medium if the electric field is perpendicular to the cleavage plane and weak if the electric field is parallel, i.e. the opposite situation to that in dioctahedral (K, Na)-micas since the O–H bond is nearer the perpendicular than the parallel direction. The Raman spectroscopic technique thus seems to be a convenient way for determining the approximate orientation of the O–H direction in the structure of dioctahedral or trioctahedral micas (cf. as determined by Serratosa and Bradley, 1958, using infrared spectroscopy).

The trilithionite samples give only a weak peak at 3691 cm^{-1}.

Trends in variation of significant Raman peaks

In this section we make some tentative evaluations of possible trends of variation of the Raman wavenumbers with the chemical compositions of these micas. The $Al^{(iv)}$, $Al^{(vi)}$ and $Al^{(tot.)}$ contents are employed as abscissae in Figs. 3–5 since they strongly influence the structural geometry of micas, and the $Al^{(tot.)}$ content is the abscissa of the 'mica hexagon' of Fig. 1 and thus represents the phengite–muscovite, phlogopite–east (K), and east (Na)-preiswerkite solid-solutions. Apart from the presence of the various minor elements, the variable proportion of Mg/(Mg + Fe) most probably also has some influence on the wavenumbers, particularly in the Fe-richer samples 12, 13, 15 and 18.

Trend of variation of the ≈195 cm^{-1} peak. Plots of the ≈195 cm^{-1} peak (Fig. 3*a*, *b* and *c*) show essentially two sub-parallel linear trends with steep slopes for the K- and Na-trioctahedral micas and one linear trend with a lower slope for dioctahedral (K)-micas. The following points merit attention:

(i) The Na-micas have a slightly higher wavenumber than their chemically-equivalent K-micas (e.g. paragonite > muscovite; east(Na) > east(K)) which can be related to the smaller ionic

size of Na^+ than K^+ which leads to a greater compaction of the Na-mica structures.

(ii) Those samples containing minor quantities of Mn^{2+}, Zn^{2+}, or Cr^{3+} are not greatly different from those of purer Mg^{2+}, Fe^{2+}, Al^{3+} end-members. Our Ti-rich annite, which is almost 2.5-octahedral, is distinctly different, with a very low wavenumber. This is certainly partly due to the larger ionic size and higher charge of Ti^{4+} compared to Al^{3+}. Note that if Ti^{4+} were added to $Al^{(vi)}$, the situation would be even more anomalous.

(iii) Trilithionite ('lepidolite') has a lower wavenumber than all the dioctahedral and trioctahedral micas except the Ti-rich annite.

(iv) F-rich phlogopite has a somewhat higher wavenumber than F-poor phlogopite.

The increasing wavenumber with increasing $Al^{(iv)}$ or $Al^{(vi)}$ conforms with Loh's (1973) interpretation that this peak involves the octahedral site, because the substitutions of Mg^{2+} by Al^{3+} in the octahedral site and of Si^{4+} by Al^{3+} in the tetrahedral site induce a shortening of the mean octahedral *M*–O bond length. The larger Al^{3+} in the tetrahedral site causes rotation of the tetrahedra, distortion of the hexagonal framework, and lengthening of the mean *T*–O bond length (Bailey, 1984*b*). The fact that Ti^{4+} and Li^+ both occupy the octahedral site and that F^- and $(OH)^-$ form part of the octahedra all agree with the octahedral site being responsible for the wavenumber of this peak. The greater intensities recorded with the electric field perpendicular to the cleavage plane imply a vibration moving the apical oxygens and (OH)/F anions mainly in the direction perpendicular to the cleavage.

Trend of variation of the ≈270 cm^{-1} peak. The K-dioctahedral micas display a sublinear trend with $Al^{(iv)}$, $Al^{(vi)}$ and $Al^{(tot.)}$ and again Na^+ causes a higher wavenumber than K^+, indeed substantially higher (Fig. 4*a*, *b* and *c*). A possible weak trend in $Al^{(vi)}$-poor K-trioctahedral micas with $Al^{(vi)}$ disappears with $Al^{(iv)}$ or $Al^{(tot.)}$, but significantly, it is apparently colinear with the trend of K-dioctahedral micas with $Al^{(vi)}$. It may be noted that preiswerkite (which has the highest octahedral charge: Mg_4Al_2) has the highest wavenumber of all and the highest intensity of this peak in trioctahedral micas. The possible trend extrapolated between trioctahedral preiswerkite (Na) and dioctahedral paragonite (Na) [and also margarite (Ca)] intersects with the apparent trend of trioctahedral plus dioctahedral K-micas in the vicinity of $Al^{(vi)} = 6$ which may be significant. If these trends are real, then the expected position of the hypothetical K-equivalent of preiswerkite around 268 cm^{-1} indicates a very large difference between K- and Na- equivalents. This does, however, fit with natural composition ranges where increasing $Al^{(tot.)}$ in trioctahedral micas from phlogopite stops around the composition east(K) because the K-equivalent of preiswerkite is unstable (Robert, 1981). Having Na instead of K changes the structure in such a way as to stabilize preiswerkite, but apparently also to greatly increase the wavenumber of the ≈270 cm^{-1} Raman peak. This does not refute the possibility that this peak is concerned with O–H–O vibrations because (OH) is on the opposite side of the tetrahedral (Al + Si) layer compared to K or Na, since replacing K by Na distorts the octahedral sites (Bailey, 1984*b*) as well as the tetrahedral sites. Since the proton is actually closer to one bridging oxygen than to the apical oxygens (Ungaretti, Smith and Tlili, in prep.) then a bridging oxygen may be involved in this peak (cf. the trifurcated hydrogen bridges OH(1)–/O4, O1, O2/ discussed by Langer *et al.*, 1981). Nevertheless, we have no specific evidence to support the role of the isosceles O–H–O triangle.

The F- or Ti-rich K-trioctahedral micas are not anomalous with regard to the possible trend with $Al^{(vi)}$ but the Li-rich micas again have very low wavenumbers.

Trend of variation of the ≈700 cm^{-1} peak. Fig. 5b and c show two distinct trends, one at high wavenumber already attributed to Si–O–Si vibration in dioctahedral K- and Na-micas and also in trioctahedral (K + Li)-mica and one imprecisely-constrained trend with lower wavenumber corresponding to Si–O–Si vibration in K- and Na-trioctahedral micas. The former trend shows slightly higher wavenumbers for Na- and (K + Li)-micas.

The situation concerning the deduced Si–O–Al vibration in the ≈650 cm^{-1} range is not yet clear, partly due to the weakness of this peak in $Al^{(vi)}$-poor micas. Nevertheless, the peak is at higher wavenumbers for trioctahedral than dioctahedral K-micas and at higher wavenumbers for Na-dioctahedral micas than their K-equivalent.

Variation in the (OH)-stretching region. The peak positions in this region are also complex due to the combined influence of *N*-, *I*- or *V*-type octahedral occupancies (Vedder, 1964; Velde, 1978; Robert and Kodama, 1988; Robert *et al.*, 1988), in- and out-of-phase effects, Al/Si ordering, and OH1/OH2 ordering (Langer *et al.*, 1981), as well as of the alkali site cation and the extent of Al substitution in octahedral and/or tetrahedral sites (Liu *et al.*, 1987). In general the *N*-type vibrations are higher in wavenumber than *I*-type which in turn are higher than *V*-type (cf. Robert and

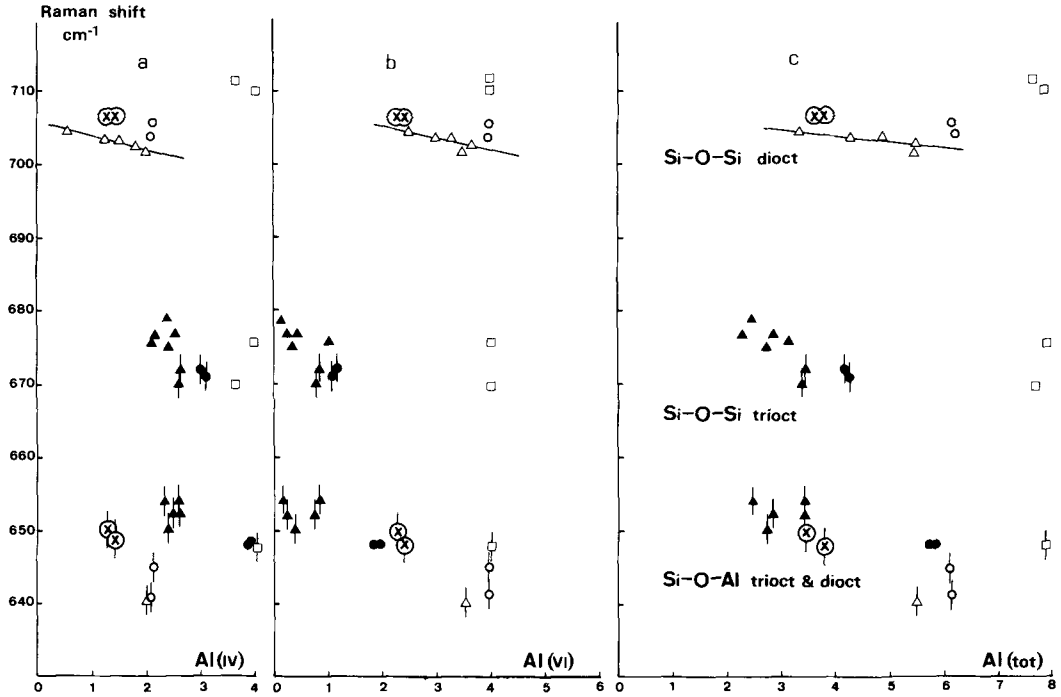

FIG. 5*a*, *b* and *c*. Trends of variation of the ≈700 cm^{-1} peak with $Al^{(iv)}$, $Al^{(vi)}$, and $Al^{(tot.)}$ respectively.

Kodama, 1988). Also, in general, *N*-type and *I*-type vibrations show decreasing wavenumber with increasing $Al^{(tot.)}$ from phlogopite to preiswerkite whereas *V*-type vibrations show increasing wavenumber with increasing Al from phengite to muscovite. As expected the intensity of *N*-type vibrations decreases with increasing $Al^{(tot.)}$ from phlogopite to preiswerkite whereas the intensity of *I*-type vibrations increases with increasing $Al^{(tot.)}$.

Concluding statement

This first systematic study of natural micas by Raman spectrometry has established that micas yield spectra which can be interpreted in terms of variation of wavenumber and intensity with variation in crystal-chemical features. At this point it is already possible to roughly determine the K-, Na-, (K + Li)- or Ca-, dioctahedral or trioctahedral, nature of an unknown mica. The next step is clearly to improve the characterization, either by obtaining a larger data set on natural micas or by examining synthetic micas with chemical compositions chosen so as:

(i) to be free of the various complicating minor elements such as F^-, Li^+, Mn^{2+}, Zn^{2+}, Cr^{3+}, Fe^{3+} or Ti^{4+}, and thus to have end-member values of the principal isovalent exchanges ($K^+ = Na^+$ and $Mg^{2+} = Fe^{2+}$); and

(ii) to substitute one cation at a time to observe the changes in Raman peak wavenumber and intensity, in particular by the exchanges: $H^+ = D^+$, $Mg^{2+} = Mn^{2+}$, $Al^{3+} = Ga^{3+}$, and $Si^{4+} = Ge^{4+}$.

A large programme of mica synthesis is, therefore, in progress and should help in clarifying the peak attributions as well as providing a basis for the chemical analysis of micas by Raman spectrometry in an analogous fashion to that now possible for multicomponent solid-solutions such as ilmenites (Pinet *et al.*, 1987) and garnets (Boyer *et al.*, 1988; Smith *et al.*, 1988) and pyroxenes (Smith, Yang and Boyer, in prep.).

Acknowledgements

This project was partially financed by a grant to Dr D. C. Smith from the Muséum National d'Histoire Naturelle ('Actions spécifiques: cristallochimie des micas'). Dr J.-L. Robert kindly commented on the manuscript and Professors P. McMillan and D. J. Vaughan provided helpful reviews.

References

Bailey, S. W. (1984*a*) Classification and structures of the micas. In *Micas* (Bailey, S. W., ed.) Reviews in Mineralogy, **13,** Min. Soc. Am., 1–12.

——(1984*b*) Crystal chemistry of the true micas. Ibid. 13–60.

Boyer, H. and Smith, D. C. (1984) Petrological applications of the Raman microprobe (RMP) to the characterisation of micron-sized minerals in eclogites. In *Microbeam Analysis 1984* (A. D. Romig and J. I. Goldstein, eds.), San Francisco, 107–10.

————Chopin, C. and Lasnier, B. (1985*a*) Raman microprobe (RMP) determinations of natural and synthetic coesite. *Phys. Chem. Minerals* **12,** 45–8.

————and Guyot, F. (1985*b*) RMP (Raman microprobe) characterisation of micron-sized run products in high P–T experimental mineralogy. *1985 Pittsburgh Conference and Exposition on Analytical Chemistry and Applied Spectroscopy* p. 1244.

——Pinet, M. and Smith, D. C. (1988) The Raman microspectrometry of synthetic garnets in the system pyrope–almandine–grossular: a new technique for the non-destructive chemical analysis of garnet microinclusions. In *11th Internat. Conf. Raman Spectroscopy (ICORS) London* (R. J. H. Clark and D. A. Long, eds.) J. Wiley, pp. 915–6.

Clemens, J. D., Sircone, S., Navrotsky, A. and McMillan, P. F. (1987) Phlogopite: High temperature solution calorimetry, thermodynamic properties, Al–Si and stacking disorder, and phase equilibria. *Geochim. Cosmochim. Acta* **51,** 2569–78.

Délé-Dubois, M.-L., Dhamelincourt, P. and Schubnel, H.-J. (1980) Etude par spectroscopie Raman d'inclusions dans les diamants, saphirs et émeraudes. *Rev. Gemm. a.f.g.* No.64, 13–6.

Donnay, G., Donnay, J. D. H. and Takeda, H. (1964) Trioctahedral one-layer micas. II. Prediction of the structure from composition and cell dimensions. *Acta Crystallogr.* **17,** 1374–81.

Farmer, V. C. (1974) The layer silicates. In *Infrared Spectra of Minerals.* (Farmer, V. C., ed.) Min. Soc. London, 539pp.

——and Velde, B. (1973) Effects of structural order and disorder on the infrared spectra of brittle micas. *Mineral. Mag.* **39,** 282–8.

Franz, G., Thomas, S. and Smith, D. C. (1986) High-pressure phengite decomposition in the Weissenstein eclogite, Munchberger Gneiss Massif, Germany. *Contrib. Mineral. Petrol.* **92,** 71–85.

Giese, Jr. R. F. (1984) Electrostatic energy models of micas. In *Micas* (Bailey, S. W., ed.) Reviews in Mineralogy **13,** Min. Soc. Am., 105–44.

Griffith, W. P. (1975) Raman spectroscopy of terrestrial minerals. In *Infrared and Raman Spectroscopy of Lunar and Terrestrial Minerals* (C. Karr, ed.) Academic Press, N.Y., pp. 299–323.

Guggenheim, S. (1984) The brittle micas. In *Micas* (Bailey, S. W., ed.) Reviews in Mineralogy **13,** Min. Soc. Am., 61–104.

——and Bailey, S. W. (1975) Refinement of margarite structure in the subgroup symmetry. *Am. Mineral.* **60,** 1023–9.

Haley, L. V., Wylie, I. W. and Koningstein, J. A. (1982) An investigation of the lattice and interlayer water vibrational spectral regions of muscovite and vermiculite using Raman microscopy. *J. Raman Spec.* **13,** 203–5.

Ishii, M., Shimanouchi, T. and Nakahira, M. (1967) Far infrared absorption spectra of layer silicates. *Inorg. Chem. Acta* **1,** 387–92.

——Nakahira, M. and Takeda, H. (1969) Far infrared absorption spectra of micas. *1969 International Clay Conference.*

Knurr, R. A. and Bailey, S. W. (1986) Refinement of Mn-substituted muscovite and phlogopite. *Clays Clay Minerals* **34,** 7–16.

Langer, K., Chatterjee, N. D. and Abraham, K. (1981) Infrared studies of some synthetic and natural 2*M*1 dioctahedral micas. *Neues Jahrb. Mineral. Abh.* **142,** 91–110.

Liu, X. F., Robert, J.-L., Bény, J.-M. and Hardy, M. (1987) Raman spectrometry of (OH) groups in synthetic trioctahedral sodium micas: comparison with infrared and thermogravimetric data. *Terra Cognita* **7,** 17.

Livi, K. J. T. and Veblen, D. R. (1987) 'Eastonite' from Easton, Pennsylvania: A mixture of phlogopite and a new form of serpentine. *Am. Mineral.* **72,** 113–25.

Loh, E. (1973) Optical vibrations in sheet silicates. *J. Phys. C: Solid State Phys.* **6,** 1091–104.

Moore, R. K. and White, W. B. (1971) Vibrational spectra of the common silicates: I. The garnets. *Am. Mineral.* **56,** 54–71.

Naumann, A. W., Safford, G. J. and Mumpton, F. A. (1966) Low-frequency (OH)-motions in layer silicate minerals. *Clays Clay Minerals* **14,** 367–83.

Ohashi, H. and Sekita, M. (1982) Raman spectroscopic study of the Si–O–Si stretching vibration in clinopyroxenes. *J. Japan. Assoc. Min. Petrol. Econ. Geol.* **77,** 455–9.

————(1983) Raman spectroscopic study of clinopyroxenes in the join $CaScAlSiO_{66}$–$CaTiAl_2O_6$. Ibid. **78,** 239–45.

Pinet, M., Smith, D. C. and Boyer, H. (1987) Raman fingerprinting of opaque and semi-opaque minerals: The natural system Geikielite–Ilmenite–Pyrophanite (GIP). *Terra Cognita* **7,** 18.

Robert, J.-L. (1981) *Etudes cristallochimiques sur les micas et les amphiboles: applications à la pétrographie et à la géochimie.* Thèse d'Etat, Université Paris XI, 206pp.

——and Gaspérin, M. (1985) Crystal structure refinement of hendricksite, a Zn- and Mn-rich trioctahedral potassium mica: a contribution to the crystal chemistry of zinc-bearing minerals. *Tscherm. Min. Petr. Mitt.* **34,** 1–14.

——and Kodama, H. (1988) Generalization of the correlations between hydroxyl-stretching wavenumbers and composition of micas in the system K_2O–MgO–Al_2O_3–SiO_2–H_2O: a single model for trioctahedral and dioctahedral micas. *Am. J. Sci.* **288**A, Wones Volume, 196–212.

——Bény, J.-M., Volfinger, M. and Monier, G. (1987) Characterization of lepidolites by Raman Spectro-

metry: examples chosen on synthetic micas. *Terra Cognita* **7,** 19.

———Bény, C. and Volfinger, M. (1988) Raman and infrared characterization of hydroxyl-lepidolites. Part I: Relationships between OH-stretching wavenumbers and compositions. *Can. Mineral.* (in press).

Rosasco, G. J. and Blaha, J. J. (1980) Raman microprobe spectra and vibrational mode assignments of talc. *Applied Spectroscopy* **34,** 140–4.

Rossman, G. R. (1984) Spectroscopy of micas. In *Micas* (Bailey, S. W., ed.) Reviews in Mineralogy **13,** Min. Soc. Am., 145–81.

Serratosa, J. M. and Bradley, W. F. (1958) Determination of the orientation of OH bond axes in layer silicates by infrared absorption. *J. Phys. Chem.* **62,** 1164–7.

Shannon, R. D. (1976) Revised effective ionic radii and systematic studies of interatomic distances in halides and chalcogenides. *Acta. Crystallogr.* **32,** 751–67.

Sharma, S. K., Simons, B. and Yoder, Jr. H. S. (1983) Raman study of anorthite, calcium Tschermak's pyroxene, and gehlenite in crystalline and glassy states. *Am. Mineral.* **68,** 1113–25.

Shimanouchi, T., Tsuboi, M. and Miyazawa, T. (1961) Optically active lattice vibrations as treated by GF-Matrix Method. *J. Chem. Phys.* **35,** 1597–612.

Smith, D. C. (1988) A review of the peculiar mineralogy of the 'Norwegian coesite-eclogite province', with crystal-chemical, petrological, geochemical, and geodynamical notes and an extensive bibliography. In *Eclogites and Eclogite-Facies Rocks* (Smith, D. C., ed.) Elsevier, Amsterdam, 1–206.

——and Boyer, H. (1985) Raman microprobe fingerprinting of ordered and disordered pyroxenes in the system diopside–omphacite–jadeite. *Terra Cognita* **5,** 429.

———(1987) An exploration of the Raman spectra of several natural high-pressure amphiboles. Ibid. **7,** 21.

——and Pinet, M. (1985) Petrochemistry of opaque minerals in eclogites from the Western Gneiss Region, Norway. II: Chemistry of the ilmenite mineral group. *Chem. Geol.* **50,** 251–66.

——Tlili, A., Boyer, H. and Bény, J.-M. (1987) Raman spectroscopy of phylloscilicates: II. Natural sodium micas, and crystal chemical comparisons with potassium micas. *Terra Cognita* **7,** 22.

——Pinet, M. and Boyer, H. (1988) Raman spectra of ternary pyralspite garnets and their preliminary calibration for the chemical analysis of synthetic or natural micron-sized crystals. Ibid. **8,** 77–8.

Tlili, A., Smith, D. C., Bény, J.-M. and Boyer, H. (1987) Raman spectroscopy of phyllosilicates: I. Natural potassium micas. Ibid. **7,** 22.

———Robert, J.-L. and Beny, J.-M. (1988) The distinction of Si–O–Si and Si–O–Al vibrations in natural and synthetic di- and tri-octahedral K-Na-micas. Ibid. **8,** 78.

Van Der Marel, H. W. and Beutelspacher, H. (1976) *Atlas of infrared spectroscopy of clay minerals and their admixtures*. Elsevier, Amsterdam.

Vedder, W. (1964) Correlations between infrared spectrum and chemical composition of mica. *Am. Mineral.* **49,** 736–68.

——and McDonald, R. S. (1963) Vibrations of the OH ions in muscovite. *J. Chem. Phys.* **38,** 1583–90.

Velde, B. (1978) Infrared spectra of synthetic micas in the series muscovite–MgAl celadonite, *Am. Mineral.* **63,** 343–9.

——and Couty, R. (1985) Far infrared spectra of hydrous layer silicates. *Phys. Chem. Minerals* **12,** 347–52.

White, W. B. (1975) Structural interpretation of lunar and terrestrial minerals by Raman spectroscopy. In *Infrared and Raman Spectroscopy of Lunar and Terrestrial Minerals* (C. Karr, ed.) Academic Press, N.Y. pp. 325–58.

——(1986) Raman spectra of silicate minerals. *14th General Meeting* International Mineralogical Association, Stanford, U.S.A.

Zussman, J. (1979) The crystal chemistry of the micas. *Bull. Mineral.* **102,** 5–13.

[*Manuscript received 1 June 1988; revised 29 July 1988*]